HVAC&R Research
Publication details, including instructions for authors and subscription information:
http://www.tandfonline.com/loi/uhvc20

Dynamic modeling of refrigerated transport systems with cooling-mode/heating-mode switch operations

Bin Li [a], Neera Jain [a], William F. Mohs [b], Scott Munns [c], Vikas Patnaik [c], Jeff Berge [b] & Andrew G. Alleyne [a]

[a] Department of Mechanical Science and Engineering, University of Illinois at Urbana-Champaign, MC-244, 1206 West Green Street, Urbana, IL, 61801, USA

[b] Department of R&D Engineering, Climate Control Technologies, Ingersoll Rand, Minneapolis, MN, USA

[c] Global Modeling & Analysis, Climate Solutions, Ingersoll Rand, La Crosse, WI, USA

Version of record first published: 27 Sep 2012.

To cite this article: Bin Li , Neera Jain , William F. Mohs , Scott Munns , Vikas Patnaik , Jeff Berge & Andrew G. Alleyne (2012): Dynamic modeling of refrigerated transport systems with cooling-mode/heating-mode switch operations, HVAC&R Research, 18:5, 974-996

To link to this article: http://dx.doi.org/10.1080/10789669.2012.670685

Dynamic modeling of refrigerated transport systems with cooling-mode/heating-mode switch operations

Bin Li,[1] Neera Jain,[1] William F. Mohs,[2] Scott Munns,[3] Vikas Patnaik,[3] Jeff Berge,[2] and Andrew G. Alleyne[1,*]

[1]*Department of Mechanical Science and Engineering, University of Illinois at Urbana-Champaign, MC-244, 1206 West Green Street, Urbana, IL 61801, USA*

[2]*Department of R&D Engineering, Climate Control Technologies, Ingersoll Rand, Minneapolis, MN, USA*

[3]*Global Modeling & Analysis, Climate Solutions, Ingersoll Rand, La Crosse, WI, USA*

[*]*Corresponding author e-mail: alleyne@illinois.edu*

This article presents dynamic modeling approaches to predict system performance characteristics of cooling-/heating-mode switch cycling operation, a commonly used temperature regulation approach in refrigerated transport systems. A dynamic model of a commercially available transport refrigeration system is presented, which describes the system dynamics during the mode switch transients. The development of the heat exchanger and accumulator models is highlighted using the switched modeling framework. Model validation against experimental data demonstrates the capabilities of the modeling approach in representing the transient behavior of the mode switch process. Simulation case studies to predict refrigerant mass distribution during transients and system performance with the influence of door-opening events are also provided to demonstrate modeling capabilities. The presented dynamic modeling framework can serve as a valuable tool to evaluate performance with different system configurations and operating strategies in transport refrigeration applications.

Introduction

Refrigerated transport systems, such as refrigerated road vehicles and refrigerated shipping containers, are widely used to distribute chilled and frozen products throughout the world. As an essential sector in the food supply cold chain, more and more attention is paid to food transport refrigeration because of increasing concerns on food safety and quality, as well as its impact on energy consumption and the environment (Tassou et al. 2009; Akkerman et al. 2010). An important characteristic of these refrigeration systems is temperature regulation so that the quality of perishable foods is preserved and the shelf life is extended during transport (James et al. 2006).

To satisfy customer needs for shipping a wide range of cargo under tight temperature control, the transport refrigeration industry has responded by improving temperature control techniques, providing greater cooling capacity, and offering load flexibility, for example, from single cargo space to

Received November 22, 2011; accepted February 9, 2012

Bin Li is PhD candidate. **Neera Jain**, Student Member ASHRAE, is PhD candidate. **William F. Mohs**, Member ASHRAE, is Senior Engineer. **Scott Munns** is Senior Engineer. **Vikas Patnaik, PhD**, Member ASHRAE, is Engineering Manager. **Jeff Berge**, Member ASHRAE, is R&D Manager. **Andrew G. Alleyne, PhD**, is Ralph M. and Catherine V. Fisher Professor.

HVAC&R Research, 18(5):974–996, 2012.
ISSN: 1078-9669 print / 1938-5587 online
DOI: 10.1080/10789669.2012.670685

multi-space systems, as noted in Vaclavek et al. (2003). Compared with stationary systems, transport refrigeration systems are required to perform reliably over a variety of operating conditions, such as broad temperature ranges of transported food products and wide variations in climatic conditions. Additionally, the refrigeration systems need to be designed to be energy efficient without compromising the temperature control of the products. To investigate and improve the refrigeration system performance, good knowledge of the system behavior is required and can be obtained either from modeling and simulation tools or through experimental studies. As mentioned in Koury et al. (2001), the use of well-verified numerical models can facilitate the understanding of system dynamic behavior, serve as a tool to evaluate alternative system designs and operating strategies, and minimize the time and expense of test-cell experiments. However, considering refrigerated transport is a complex interacting system, complete understanding of dynamic models to predict the system thermodynamic behavior is still lacking, and many efforts have been dedicated to improve predictive capabilities (James et al. 2006; Jolly et al. 2000).

This present study develops a specific modeling approach to simulate common operations in refrigerated transport applications: cooling-/heating-mode switch cycling operations (Tso et al. 2001; Repice and Stumpf 2007). Different from cycling the refrigeration systems on and off for temperature regulation (Li et al. 2010), in cooling-/heating-mode switch operation, the product temperature is maintained at a set-point below the ambient conditions by continuously running the system and cycling between cooling and heating modes. One reason to drive the refrigeration equipment to switch from cooling to heating mode is the need for defrosting the heat exchangers (Hoffenbecker et al. 2005; Dopazo et al. 2010). Another reason is to maintain a continuous supply of air moving over the transported food product, which is a requirement for fresh produce (e.g., strawberries). The cooling-/heating-mode switch allows for temperature regulation while maintaining continuous air circulation.

It is challenging to simulate the mode switch cycling operation since it is a complex and highly transient process involving component function variations as well as many indeterminate variables (Krakow et al. 1993). From the open literature in heat pump applications, there have been extensive experimental investigations of system performance during the switch between normal operating mode and defrosting mode. These include reverse-cycle defrosting processes (Miller 1987; O'Neal et al. 1989; Qu et al. 2012) and hot-gas bypass defrosting methods (Cho et al. 2005; Byun et al. 2008). Nevertheless, there are few studies on the development of simulation models to predict the system dynamics under normal-/defrosting-mode switch cycling operation. Krakow et al. (1993) developed an analytical reverse-cycle defrosting model where the melting process on the coil surface was idealized by subdividing it into different stages. Based on the above modeling theory, Liu et al. (2003) presented a validated reverse-cycle defrosting model for an air-source heat pump system. While the defrost process is important, this article focuses on the development of capabilities to simulate the mode switch cycle operation for temperature regulation in transport refrigeration, rather than detailing the frost melting mass and heat transfer process involved in the defrosting mechanism.

To investigate the dynamic behavior of refrigeration systems, heat exchangers are usually treated with transient models. Two common heat exchanger modeling approaches, finite-volume and moving-boundary methods, have been reported in the literature (He et al. 1997; Jensen and Tummescheit 2002; Bendapudi and Braun 2002; Rasmussen and Alleyne 2004; Bendapudi et al. 2005; Eborn et al. 2005; Limperich et al. 2005). Liu et al. (2003) used distributed-parameter finite-volume models for the condenser and evaporator during the defrosting cycle. Bendapudi et al. (2008) compared the two approaches in predicting system start-up and load change transients in a centrifugal chiller application, while Kapadia et al. (2009) applied the finite-volume approach to analyze the start-up performance of a split air-conditioning system. A switched moving-boundary framework was demonstrated in Li and Alleyne (2010) to simulate system shut-down and start-up performance. In this framework, the heat exchangers were developed with different model representations to accommodate the transitions of dynamic states during transients. Jain (2009) developed cooling-mode and heating-mode operation dynamic models for a commercial transport refrigeration unit, where the moving-boundary modeling approach was applied. On the basis of the switched modeling framework (Li and Alleyne 2010) and the transport refrigeration models (Jain 2009), this article models the single cargo space transport refrigeration system, validates the system

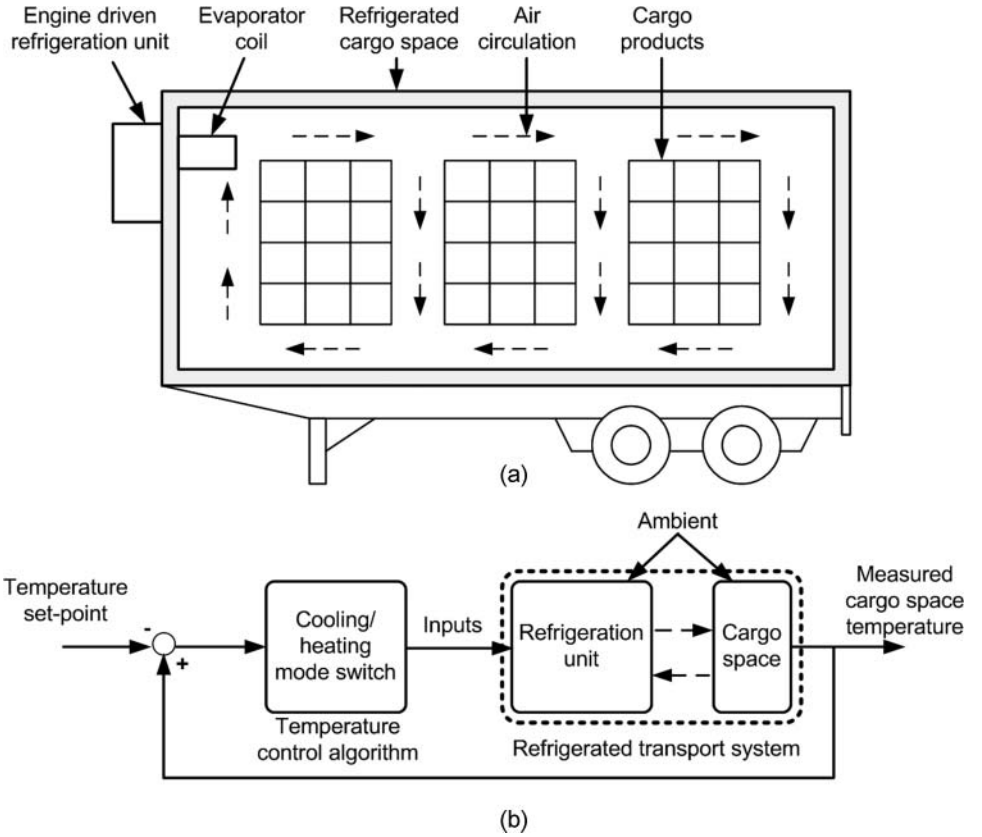

Figure 1. (a) A typical single cargo space refrigerated transport system and (b) schematic of cooling-/heating-mode switch temperature control system.

dynamic characteristics during cooling-/heating-mode switch cycles, and predicts refrigerant mass distribution among the system components in transients.

The rest of this article is organized as follows. The "Experimental refrigeration system" section describes the switching operation between cooling and heating mode in the experimental transport refrigeration system as well as the process through which data is acquired for the system model validation. The "System modeling" section introduces the modeling of individual components that are active during either the cooling or the heating mode of operation. Using the switched modeling framework in Li and Alleyne (2010), the heat exchanger components are modeled to capture the transients during cooling-/heating-mode switch cycles. Model validation results are presented in the section entitled "Model validation" to demonstrate the capabilities of the developed model in predicting system dynamics during mode switch cycling. Finally, a simulation case study for temperature regulation in a transport refrigeration unit involving door-opening events is given in the "Case study" section. A conclusion section summarizes the main points of the article.

Experimental refrigeration system

As indicated in Figure 1a, a typical refrigerated transport system consists of a refrigeration unit and a refrigerated cargo space. The refrigeration unit is interacting with the cargo space to meet its temperature requirements and satisfy the refrigeration demands over a wide range of operating conditions (Tassou et al. 2009). Under a cooling-/heating-mode switch operation scheme for temperature regulation (see Figure 1b), the system operation mode (cooling or heating) is driven by the difference between measured cargo space temperature and the temperature set-point. The cargo space is coupled to the refrigeration unit such that the cargo space outputs,

e.g., return air temperature (normally considered as the cargo space temperature), are the inputs to the refrigeration unit, e.g., evaporator air inlet temperature. Simultaneously, the refrigeration unit outputs, e.g., evaporator air outlet temperature, are acting as the cargo space inputs, e.g., supply air temperature. As mentioned earlier, the heat exchanger fans are continuously running during mode switch cycling.

The dual-mode refrigeration system studied in this article is a commercially available TS-500 transport refrigeration unit manufactured by Thermo King Corporation. The refrigeration system is charged with refrigerant R404A. The primary mode of operation is the cooling cycle in which the unit extracts heat from the refrigerated cargo space and transfers it to the external ambient environment. In the second mode of operation, the heating cycle, the refrigeration unit delivers heat to the cargo space. Figure 2 shows a schematic of the system configuration where components are interconnected to form a vapor compression cycle (VCC) refrigeration system. The switch from cooling mode to heating mode is completed using a three-way valve that directs the path of the refrigerant exiting the compressor toward the evaporator through the discharge pressure regulator (DPR) valve rather than to the condenser coil, as can be seen in Figure 2. In heating-mode operation, the refrigerant between the condenser inlet and the thermostatic expansion valve (TXV) outlet is trapped if the valve bleed port effect is not considered. The refrigerant flows through the hot gas line to the evaporator coil. The evaporator now functions as a condenser, taking superheated vapor in and condensing it into two-phase fluid while heating the cargo space. After separation in the accumulator, the saturated refrigerant vapor passes through the throttle valve and finally returns to the compressor. Once the measured cargo space temperature exceeds the upper limit of the cargo space temperature set-point, the unit switches from heating- to cooling-mode operation, where the superheated refrigerant vapor exiting the compressor is redirected by the three-way valve to the condenser coil. A representative pressure-enthalpy (P-h) diagram for cooling- and heating-mode operation is plotted in Figure 3, where refrigerant pressures along the heat exchanger coils are assumed to be uniform.

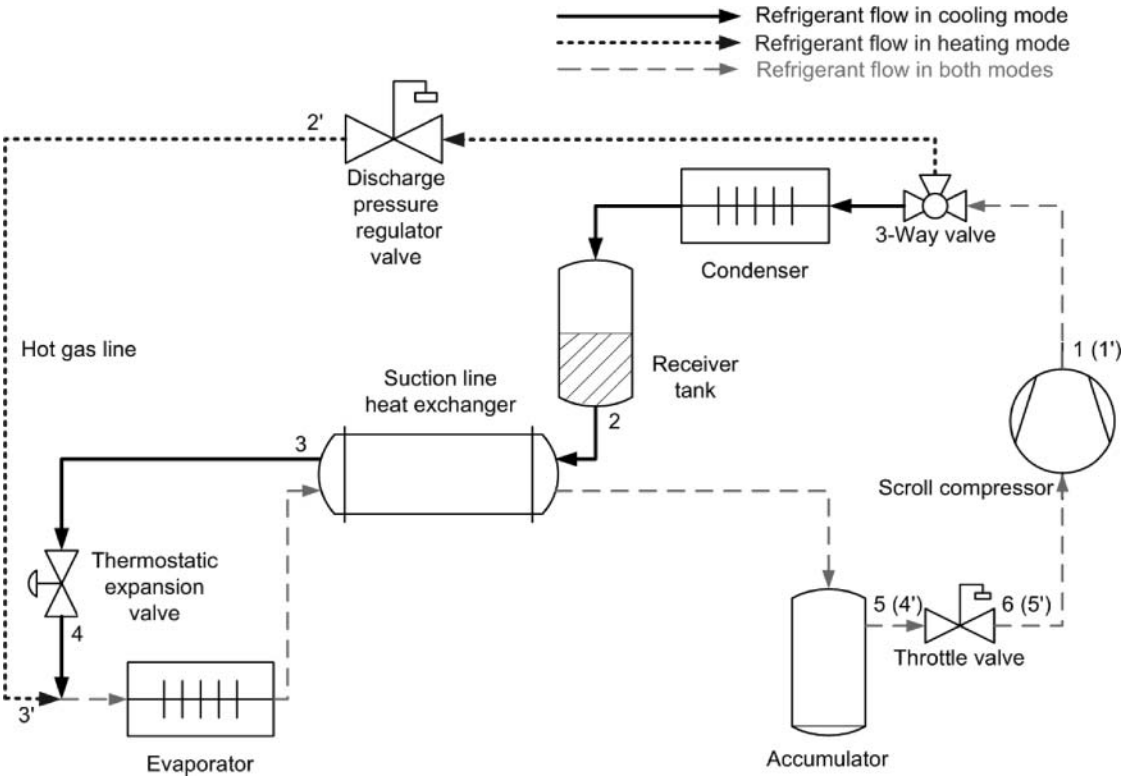

Figure 2. Schematic of the refrigeration unit in operation.

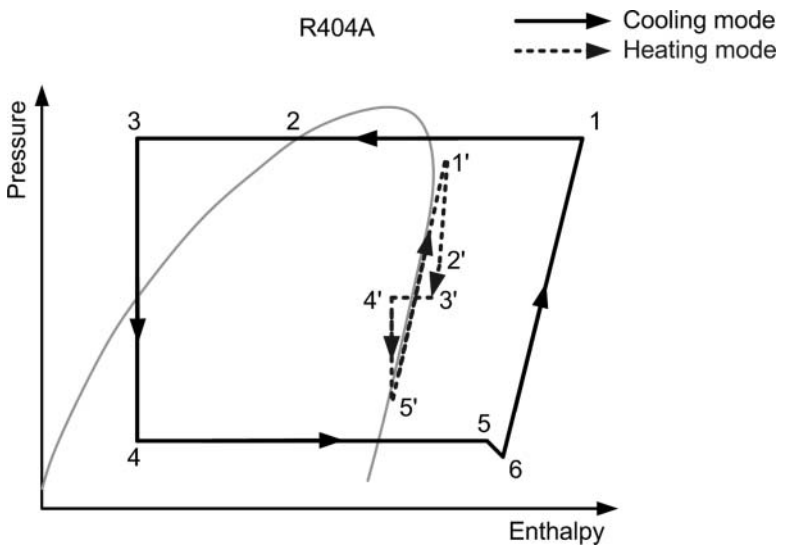

Figure 3. P-h diagram for cooling and heating mode.

All experimental data presented in this article were collected at the Thermo King Corporation test facility located in Minneapolis, Minnesota, USA. The experimental refrigeration system as shown in Figure 4 was instrumented with type-T thermocouples and pressure transducers. Air temperatures entering and leaving the heat exchangers were measured with thermocouple grids placed near the coils. Immersion thermocouples were used to monitor the refrigerant temperature at different locations in the refrigeration unit. Four thermocouple stands (see Figure 4b) were used for measuring the air temperature profile inside the cargo space. Table 1 presents the accuracy of sensors in measurements. Along with the status of each solenoid valve in the refrigeration system, each temperature sensor and pressure transducer was connected to an Agilent 34970A data acquisition system to observe the system behavior during testing. The temperature and pressure measurements were collected every 10 sec.

The experimental scenario involved a temperature pull-down and control test for the enclosed cargo space. The test procedure can be described as a "high speed pull-down of the cargo space temperature from ambient temperature to a given set-point (fresh or frozen) using the refrigeration unit; then continuously run cooling-/heating-mode switch cycle operation with low speed to maintain the space temperature." The experimental results are used to validate the dynamic model discussed in the following sections. The reader is encouraged to refer to Jain (2009) for more information regarding

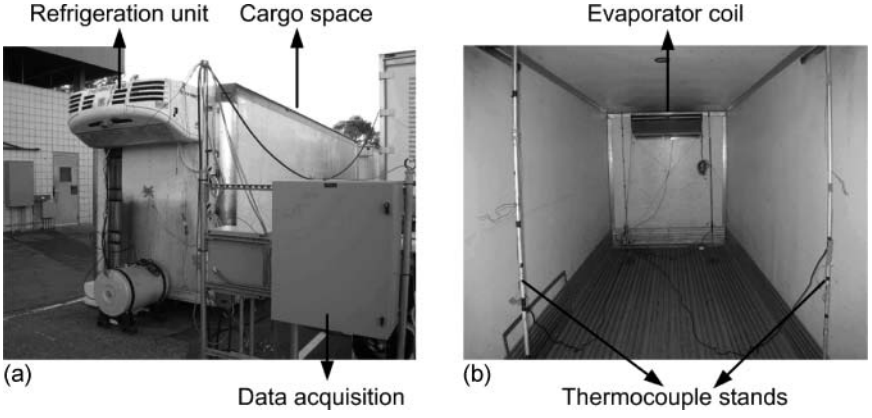

Figure 4. (a) Photograph of the experimental system and (b) instrumentation inside the cargo space.

Table 1. Locations and accuracy of sensors.

Sensor	Accuracy
Type-T thermocouples for air and refrigerant temperature	±0.5°C (0.9°F)
Pressure transducer at compressor discharge side	±10 kPa (1.45 psi)
Pressure transducer at compressor suction side	±10 kPa (1.45 psi)
Pressure transducer at receiver tank outlet	±10 kPa (1.45 psi)
Pressure transducer at evaporator outlet	±10 kPa (1.45 psi)

cooling- and heating-mode operation as well as instrumentation of the refrigeration unit.

System modeling

This section is divided into three parts. The refrigeration unit model (see Figure 2) is presented first, where the main component models are introduced. The evaporator and accumulator models are the key components operating in both cooling and heating modes. They are presented here to capture the mode switch transient performance using the switched modeling framework (Li and Alleyne 2010). Second, a dynamic refrigerated cargo space model is given based on the heat balance processing method (Li et al. 2010). Combining the unit and cargo space models, the overall transport refrigeration system can be represented for the simulation and validation studies discussed in the "Model validation" and "Case study" sections. The third part of this section illustrates the simulation environment.

Refrigeration unit model development

As discussed in Jain (2009), the refrigeration unit system depicted in Figure 2 includes static components and dynamic components. The static components (i.e., compressor, regulation valves, and suction line heat exchanger [SLHX]) are modeled using steady-state equations under the assumption that the dynamics of these components are generally an order of magnitude faster than those of the dynamic components (i.e., heat exchangers, receiver tank, and accumulator) and, therefore, less dominant in the overall system. As can be seen in Figure 2, the VCC refrigeration system is subdivided into three component portions to represent the variations in mode operations, and each portion is discussed in what follows. More descriptions about the individual component models of the refrigeration unit operating in cooling and heating mode can be found in Jain (2009).

Common components in both modes

Evaporator: When the system switches from cooling- to heating-mode operation, the evaporator acts like a condenser. Specifically, superheated vapor enters the evaporator coil and exits as two-phase fluid. When the system switches back to cooling-mode operation, the evaporator starts to extract heat again from the cargo space. There have been many studies investigating switched evaporator model development (Li and Alleyne 2010; Pettit et al. 1998; Zhang and Zhang 2006; Shao and Zhang 2007; Liang et al. 2010; Cecchinato and Mancini 2011). They focused on performance prediction with the appearance and disappearance of the superheated zone at the evaporator outlet upon varying conditions, and the refrigerant entering the evaporator was always assumed to be a two-phase or subcooled fluid.

Using the switched moving-boundary modeling framework presented by Li and Alleyne (2010), the evaporator can be extended to accommodate three different model representations (see Figure 5) to capture system transient behavior during cooling-/heating-mode switching. The two-zone (two-phase and superheated) or the one-zone (two-phase) evaporator model in Figure 5 can be used to describe the evaporator performance in cooling mode, while another two-zone (superheated and two-phase) model represents the evaporator coil when the system is running in heating mode.

The dynamic state vector in Equation 1 defines the evaporator conditions (i.e., pressure, enthalpy, temperature, and zone locations) at each instant in time. The pseudo-state technique (Li and Alleyne 2010; McKinley and Alleyne 2008b) is applied to maintain a uniform state vector, independent of model representations. Each model representation is formulated in a nonlinear descriptor form in Equation 2, as in Rasmussen (2005), with the uniform state vector x_e. The coefficient matrix $z(x_e, u_e)$ contains thermodynamic variables, and $f(x_e, u_e)$ is a forcing function containing mass and energy

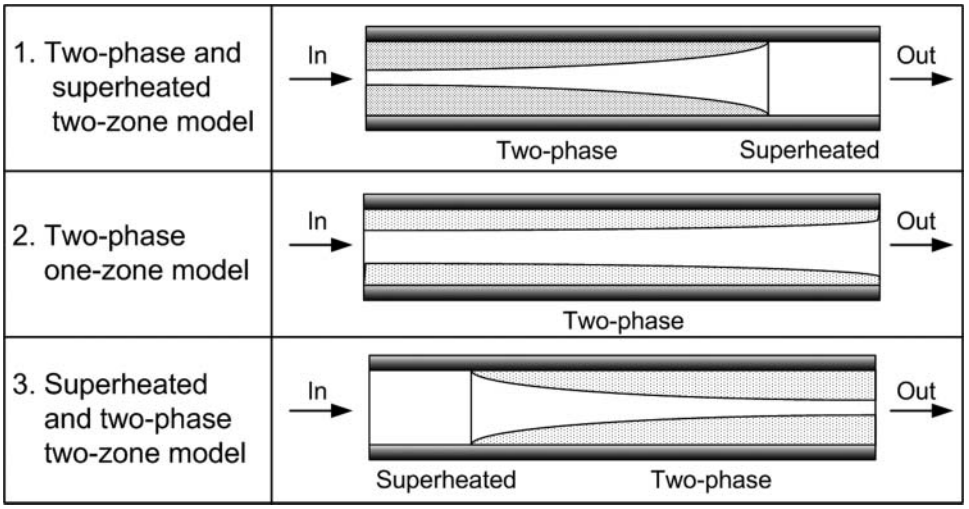

Figure 5. Switched evaporator model structure.

balance terms. The interested reader is referred to Rasmussen (2005) for a more complete modeling definition of the matrix $z(x_e, u_e)$ and the function $f(x_e, u_e)$. An advantage of this switched approach is the tracking of the vapor and liquid refrigerant dynamic states in numerical simulation while ensuring refrigerant mass conservation during switches among different model representations (Li et al. 2011):

$$x_e = [h_{e0}\ P_e\ h_{e2}\ \zeta_{e0}\ \zeta_{e1}\ T_{e0,w} T_{e1,w}\ T_{e2,w}\ \bar{\gamma}_e]^T, \quad (1)$$

$$z(x_e, u_e) \cdot \dot{x}_e = f(x_e, u_e), \quad (2)$$

$$T_{o,air,j} = T_{w,j} + (T_{i,air} - T_{w,j} \exp(-NTU)), \quad (3)$$

$$NTU = \frac{\alpha_{air} A_{air} \left(1 - \frac{A_{fin}}{A_{air}} (1 - \eta_{fin,air})\right)}{\dot{m}_{air} c_{air}}. \quad (4)$$

Besides the modeling assumptions given in Li and Alleyne (2010), additional assumptions are made as follows.

A. The evaporator is assumed to be a long horizontal single-pass tube with a mass flow rate reduced by a factor of $1/n$, where n is the number of evaporator circuits (in this study, n is equal to 11). Furthermore, relevant physical parameters, such as heat exchanger mass and airflow cross-sectional area, are reduced by the same factor (Jain 2009).
B. The two-phase slip flow can be modeled adequately through a void fraction correlation (Zivi 1964).
C. The air passing over the evaporator is assumed to be in dry conditions, and the effects of water vapor condensation on the system performance are not taken into account.

The NTU method is applied to represent the relationship between air inlet and outlet temperature in the evaporator, as shown in Equations 3 and 4 and demonstrated in McKinley and Alleyne (2008b). The evaporator structure governing equations involving the calculations of the structure-to-air and structure-to-refrigerant heat transfer rates were discussed in Li and Alleyne (2010). The refrigerant-side governing equations are derived by considering mass and energy conservation in each zone (i.e., superheated zone, two-phase zone). Only the final forms of the governing equations for the three model representations (see Figure 5) as well as switching criteria are shown here.

1. **Two-phase and superheated two-zone model.** In this representation, the inlet refrigerant to the evaporator is a two-phase fluid. Equations 5 and 6 describe the two-phase refrigerant dynamics, and the mass and energy conservation equations for the superheated zone are given in Equations 7 and 8. The mean void fraction equation (Equation 9) is also included in this model for

switching purposes (Li and Alleyne 2010):

$$\frac{d\zeta_{e1}}{dt}+\frac{\zeta_{e1}}{\rho_{e1}}\frac{\delta\rho_{e1}}{\delta P_e}\frac{dP_e}{dt}+\frac{\zeta_{e1}}{\rho_{e1}}\frac{\delta\rho_{e1}}{\delta\bar{\gamma}_e}\frac{d\bar{\gamma}_e}{dt}+\frac{\dot{m}_{e12}}{\rho_{e1}V_e}=\frac{\dot{m}_{i,e}}{\rho_{e1}V_e}, \tag{5}$$

$$\left[\frac{\delta h_{e1}}{\delta P_e}-\frac{1}{\rho_{e1}}\right]\frac{dP_e}{dt}+\frac{\delta h_{e1}}{\delta\bar{\gamma}_e}\frac{d\bar{\gamma}_e}{dt}+\frac{h_{e,g}-h_{e1}}{\rho_{e1}V_e\zeta_{e1}}\dot{m}_{e12}=\frac{\dot{Q}_{e1}+\dot{m}_{i,e}(h_{i,e}-h_{e1})}{\rho_{e1}V_e\zeta_{e1}}, \tag{6}$$

$$\frac{d\zeta_{e1}}{dt}-\frac{\zeta_{e2}}{\rho_{e2}}\frac{\delta\rho_{e2}}{\delta P_e}\frac{dP_e}{dt}-\frac{\zeta_{e2}}{\rho_{e2}}\frac{\delta\rho_{e2}}{\delta h_{e2}}\frac{dh_{e2}}{dt}+\frac{\dot{m}_{e12}}{\rho_{e2}V_e}=\frac{\dot{m}_{o,e}}{\rho_{e2}V_e}, \tag{7}$$

$$-\frac{1}{\rho_{e2}}\frac{dP_e}{dt}+\frac{dh_{e2}}{dt}-\frac{h_{e,g}-h_{e2}}{\rho_{e2}V_e\zeta_{e2}}\dot{m}_{e12}=\frac{\dot{Q}_{e2}-\dot{m}_{o,e}(h_{e2}-h_{e,g})}{\rho_{e2}V_e\zeta_{e2}}, \tag{8}$$

$$\frac{\delta\bar{\gamma}_{etot}}{\delta P_e}\frac{dP_e}{dt}-\frac{d\bar{\gamma}_e}{dt}=K(\bar{\gamma}_e-\bar{\gamma}_{etot}). \tag{9}$$

Since the superheated zone at the evaporator inlet is made inactive in this model representation, Equation 10 is applied, and the state equation for the refrigerant enthalpy in this zone is described in Equation 11. The pseudo-state equation (Equation 12) is used to govern the evaporator structure behavior for the inactive superheated zone, which tracks the wall temperature of the active two-phase zone:

$$\frac{d\zeta_{e0}}{dt}=0, \tag{10}$$

$$\frac{dh_{e0}}{dt}=\frac{1}{2}\frac{dh_{i,e}}{dt}+\frac{1}{2}\frac{\delta h_{e,g}}{\delta P_e}\frac{dP_e}{dt}, \tag{11}$$

$$\frac{dT_{e0,w}}{dt}=K(T_{e1,w}-T_{e0,w}). \tag{12}$$

2. **Two-phase one-zone model.** Due to the disappearance of the superheated zone at the evaporator outlet, the pseudo-state equation (Equation 13) causes the superheated zone refrigerant enthalpy to track the saturated vapor enthalpy, and Equation 14 is used to govern the wall temperature in this inactive superheated zone by tracking the active two-phase zone state. The constant length of the only active two-phase zone is described in Equation 15, and Equations 10–12 still apply to represent the inactive superheated zone states at the evaporator inlet:

$$\frac{dh_{e2}}{dt}=K(h_{e,g}-h_{e2}), \tag{13}$$

$$\frac{dT_{e2,w}}{dt}=K(T_{e1,w}-T_{e2,w}), \tag{14}$$

$$\frac{d\zeta_{e1}}{dt}=0. \tag{15}$$

The refrigerant-side mass and energy conservation equations for this two-phase zone become

$$\frac{\zeta_{e1}}{\rho_{e1}}\frac{\delta\rho_{e1}}{\delta P_e}\frac{dP_e}{dt}+\frac{\zeta_{e1}}{\rho_{e1}}\frac{\delta\rho_{e1}}{\delta\bar{\gamma}_e}\frac{d\bar{\gamma}_e}{dt}=\frac{\dot{m}_{i,e}-\dot{m}_{o,e}}{\rho_{e1}V_e}, \tag{16}$$

$$\left[\frac{\delta h_{e1}}{\delta P_e}-\frac{1}{\rho_{e1}}\right]\frac{dP_e}{dt}+\frac{\delta h_{e1}}{\delta\bar{\gamma}_e}\frac{d\bar{\gamma}_e}{dt}=\frac{\dot{Q}_{e1}+\dot{m}_{i,e}(h_{i,e}-h_{e1})-\dot{m}_{o,e}(h_{o,e}-h_{e1})}{\rho_{e1}V_e\zeta_{e1}}. \tag{17}$$

3. **Superheated and two-phase two-zone model.** When the system switches to the heating mode of operation, the evaporator behaves as a condenser, condensing the inlet superheated vapor into two-phase refrigerant. The mass and energy equations (Equations 18 and 19), along with the refrigerant enthalpy state equation (Equation 11), are used to describe the refrigerant dynamics for the inlet superheated zone. The conservation equations for the two-phase zone are shown in Equations 20 and 21:

$$\frac{d\zeta_{e0}}{dt}+\frac{\zeta_{e0}}{\rho_{e0}}\frac{\partial\rho_{e0}}{\partial P_e}\frac{dP_e}{dt}+\frac{\zeta_{e0}}{\rho_{e0}}\frac{\partial\rho_{e0}}{\partial h_{e0}}\frac{dh_{e0}}{dt}+\frac{\dot{m}_{e01}}{\rho_{e0}V_e}=\frac{\dot{m}_{i,e}}{\rho_{e0}V_e}, \tag{18}$$

$$\frac{dh_{e0}}{dt}-\frac{1}{\rho_{e0}}\frac{dP_e}{dt}+\frac{(h_{e,g}-h_{e0})}{\rho_{e0}V_e\zeta_{e0}}\dot{m}_{e01}=\frac{\dot{Q}_{e0}+\dot{m}_{i,e}(h_{i,e}-h_{e0})}{\rho_{e0}V_e\zeta_{e0}}, \tag{19}$$

$$-\frac{d\zeta_{e0}}{dt}+\frac{\zeta_{e1}}{\rho_{e1}}\frac{\partial\rho_{e1}}{\partial P_e}\frac{dP_e}{dt}-\frac{\dot{m}_{e01}}{\rho_{e1}V_e}+\frac{\zeta_{e1}}{\rho_{e1}}\frac{\partial\rho_{e1}}{\partial\bar{\gamma}_e}\frac{d\bar{\gamma}_e}{dt}=-\frac{\dot{m}_{o,e}}{\rho_{e1}V_e}, \tag{20}$$

$$\left[\frac{\partial h_{e1}}{\partial P_e}-\frac{1}{\rho_{e1}}\right]\frac{dP_e}{dt}-\frac{(h_{e,g}-h_{e1})}{\rho_{e1}V_e\zeta_{e1}}\dot{m}_{e01}+\frac{\partial h_{e1}}{\partial \bar{\gamma}_e}\frac{d\bar{\gamma}_e}{dt} = \frac{\dot{Q}_{e1}-\dot{m}_{o,e}(h_{o,e}-h_{e1})}{\rho_{e1}V_e\zeta_{e1}}. \quad (21)$$

Since the refrigerant superheated zone at the evaporator outlet is inactive, Equation 22 is applied. With the pseudo-state equations (Equations 13 and 14), the dynamic states of this superheated zone are forced to track the corresponding states of the active zone:

$$\frac{d\zeta_{e0}}{dt}+\frac{d\zeta_{e1}}{dt}=0. \quad (22)$$

4. **Switching criteria.** Refrigerant mass conservation is the major concern when choosing the switching criteria among different model representations (Li and Alleyne 2010; Cecchinato and Mancini 2011; McKinley and Alleyne 2008b). Switching conditions between the two-zone (two-phase and superheated) and the one-zone (two-phase) evaporator model were presented in Li and Alleyne (2010), with the assumption that the inlet refrigerant to the evaporator is a two-phase fluid. Specifically, the conditions to trigger the switch from the one-zone to the two-zone (two-phase and superheated) evaporator model are given in Equations 23 and 24:

$$\zeta_{e1}(\bar{\gamma}_e-\bar{\gamma}_{etot})>\zeta_{e\min}, \quad (23)$$

$$\frac{d\bar{\gamma}_e}{dt}>0. \quad (24)$$

If the mean void fraction $\bar{\gamma}_e$ is above the equilibrium value for evaporation to saturated vapor, the term inside parentheses in Equation 23 will be positive. This means that there is excess vapor volume in the two-phase zone. The term on the left side of Equation 23 represents the normalized length of excess vapor volume, and $\zeta_{e\min}$ on the right side is regarded as a tunable switching threshold indicating the minimum dimensionless length of the superheated zone within the total evaporator tube length. The value of this threshold is chosen to be 0.001 as a starting point (Li and Alleyne 2010). Therefore, these conditions can be stated as "the existence and further increase of excess vapor volume in the two-phase zone indicate the occurrence of a superheated vapor zone at the evaporator outlet."

Switching from the one-zone (two-phase) to another two-zone (superheated and two-phase) model representation could occur when the system operation transitions from cooling to heating mode, and the conditions are defined as follows:

$$h_{i,e}>h_{e,g}, \quad (25)$$

$$\frac{dh_{i,e}}{dt}>0. \quad (26)$$

If the inlet refrigerant enthalpy is above the saturated vapor enthalpy value, Equation 25 will be satisfied. This means the superheated refrigerant vapor enters the evaporator. So, these conditions can be explained as "the inlet refrigerant in the evaporator becomes superheated vapor and the inlet enthalpy is continuing to increase."

Similarly, switching back to cooling-mode operation could drive the evaporator to switch from the two-zone (superheated and two-phase) to the one-zone model when the switching conditions given in Equations 27 and 28 are satisfied:

$$h_{i,e}<h_{e,g}, \quad (27)$$

$$\frac{dh_{i,e}}{dt}<0. \quad (28)$$

SLHX: The SLHX is a refrigerant liquid to refrigerant vapor heat exchanger. The thermal capacitance of the SLHX is assumed to be small in comparison to that of the evaporator and condenser; therefore, the associated dynamics can be treated as static. In cooling-mode operation, hot refrigerant liquid exiting the receiver tank flows through the inner coil of the SLHX, where it loses heat to the cold refrigerant vapor flowing through the outer shell of the SLHX. During heating mode, the two-phase refrigerant exiting the evaporator passes through the outer shell of the SLHX without undergoing significant heat transfer due to the trapped refrigerant in the inner coil. The reader is referred to Jain (2009) for details on this component model.

Accumulator: The accumulator is a device normally used to separate vapor from liquid in two-phase flow, thus preventing damage to the compressor. When the system is in cooling mode of operation, due to the presence of the SLHX in the refrigerant circuit, the refrigerant entering the accumulator is superheated vapor, and the accumulator acts as a superheated vapor tank with heat transfer characteristics. However, since the

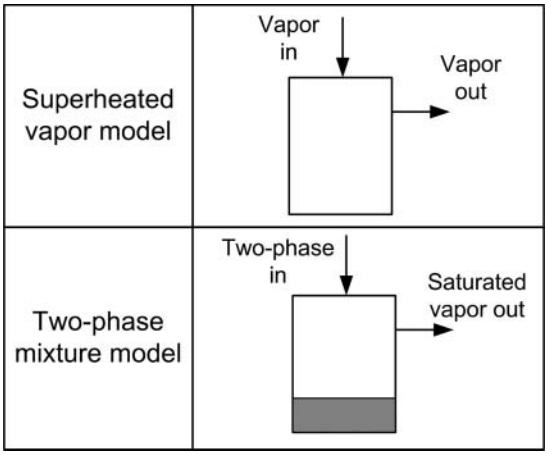

Figure 6. Switched accumulator model structure.

evaporator behaves like a condenser in heating mode, refrigerant liquid accumulates at the bottom of the accumulator, and saturated refrigerant vapor flows out of the accumulator tank. Therefore, in this study, the accumulator is developed with two model representations, as shown in Figure 6.

Two dynamic states, refrigerant pressure P_{ac} and average refrigerant enthalpy h_{ac}, are defined to describe the refrigerant dynamics inside the accumulator for both representations. The structure of refrigerant-side mass and energy governing equations in each model representation is the same and is given below:

$$\frac{\delta\rho_{ac}}{\delta P_{ac}}\frac{dP_{ac}}{dt}+\frac{\delta\rho_{ac}}{\delta h_{ac}}\frac{dh_{ac}}{dt}=\frac{\dot{m}_{i,ac}-\dot{m}_{o,ac}}{V_{ac}}, \tag{29}$$

$$-\frac{1}{\rho_{ac}}\frac{dP_{ac}}{dt}+\frac{dh_{ac}}{dt}=\frac{(UA)_{ac}(T_{amb}-T_{ac})+\dot{m}_{i,ac}(h_{i,ac}-h_{ac})-\dot{m}_{o,ac}(h_{o,ac}-h_{ac})}{\rho_{ac}V_{ac}}, \tag{30}$$

where the term $(UA)_{ac}(T_{amb}-T_{ac})$ represents the heat transfer rate from the ambient air to the refrigerant inside the accumulator; the calculations of the heat transfer coefficients $(UA)_{ac}$ in cooling and heating mode are available in Jain (2009). The difference in the governing equations between the two representations is the exiting refrigerant enthalpy $h_{o,ac}$ in Equation 30. In the two-phase mixture model, the exiting refrigerant is saturated vapor, while the exiting enthalpy is assumed to be the average enthalpy h_{ac} in the superheated vapor model representation (Zhang et al. 2009).

The accumulator model switching criteria are determined based on the mean void fraction $\bar{\gamma}_{ac}$, which is defined as the ratio of refrigerant vapor volume to total volume, and can be represented as a function of the refrigerant pressure P_{ac} and the refrigerant enthalpy h_{ac}. For example, the switch occurs from the two-phase mixture model to the superheated vapor model when the switching conditions, as given in Equations 31 and 32, are satisfied:

$$\bar{\gamma}_{ac} > 1, \tag{31}$$

$$\frac{dh_{ac}}{dt} > 0. \tag{32}$$

If the mean void fraction value is above one as shown in Equation 31, this means the accumulator is filled with vapor and the average refrigerant enthalpy is above the saturated vapor enthalpy. So, these switching conditions can be stated as "the refrigerant enthalpy inside the accumulator becomes larger than the saturated vapor enthalpy and continues to increase."

When the system operation switches from cooling to heating mode, the conditions to trigger the switch from the superheated vapor accumulator to the two-phase mixture model are explained in Equations 33 and 34:

$$\bar{\gamma}_{ac,calc} < 1, \tag{33}$$

$$\frac{dh_{ac}}{dt} < 0. \tag{34}$$

The mean void fraction $\bar{\gamma}_{ac,calc}$ in the superheated vapor model is calculated in Equation 35. If this value is below one, the average refrigerant quality $\tilde{x}_{ac}$ inside the accumulator will be below one, and Equation 33 will be satisfied. This means the refrigerant enthalpy is below the saturated vapor enthalpy, and there is excess liquid volume accumulating at the bottom. Therefore, these conditions can be described as "the mean void fraction indicates there is noticeable excess liquid volume inside the accumulator superheated vapor model and it continues to accumulate":

$$\bar{\gamma}_{ac,calc}=\frac{\tilde{x}_{ac}\rho_{ac,f}}{\tilde{x}_{ac}\rho_{ac,f}+(1-\tilde{x}_{ac})\rho_{ac,g}}. \tag{35}$$

Throttle valve: The throttle valve, also known as a suction pressure regulator valve, is a mechanical

control valve to regulate the pressure of the refrigerant vapor at the compressor inlet. This valve model is developed using an empirical map that was presented in Jain (2009).

Scroll compressor: The TS-500 refrigeration unit contains an open-drive scroll compressor. The compressor is operated using a diesel engine and can run at three speeds, denoted as high speed, low speed, and null (approximately 4000, 2500, and 0 rpm, respectively). The compressor mass flow rate is computed using

$$\dot{m}_k = V_k \omega_k \rho_k \eta_{vol}, \tag{36}$$

where V_k is the cylinder volume, ω_k is the compressor speed, and ρ_k is the refrigerant inlet density. The volumetric efficiency η_{vol} is calculated using a performance mapping approach provided in Jain (2009).

Components in cooling mode

Condenser: As mentioned previously, when the system shifts from cooling- to heating-mode operation, the refrigerant flow is redirected by the three-way valve (see Figure 2) to the hot gas line rather than to the condenser coil. In this scenario, the condenser acts as if the system were "shutting down," where the remaining refrigerant inside the coil continues to flow out of the condenser and enters the receiver tank due to the inertia and pressure differential. Therefore, the switched condenser modeling framework to handle system shut-down transients (Li and Alleyne 2010; McKinley and Alleyne 2008b) is applied here for the condenser operating in cooling mode. Detailed descriptions of the model governing equations were presented in McKinley and Alleyne (2008b).

Receiver tank: The primary function of the receiver tank in the refrigeration system is to store excess refrigerant mass to ensure system capacity over a large range of operating conditions. The structure of the refrigerant-side mass and energy governing equations for the receiver component is similar to Equations 29 and 30, and the exiting refrigerant is assumed to be saturated liquid.

TXV: As another mass flow device in the system, in cooling-mode operation, the TXV controls the refrigerant mass flow entering the evaporator by maintaining a certain level of refrigerant superheat at the evaporator outlet. Equation 37 is used to calculate the mass flow rate, where the flow coefficient C_f is determined via a semi-empirical mapping approach (Li 2009):

$$\dot{m}_v = C_f \sqrt{\rho_v (P_{o,slhx} - P_e)}. \tag{37}$$

In heating-mode operation, the disappearance of superheat at the evaporator outlet results in the closed position of the expansion valve; however, the bleed port effect of the TXV is modeled by assuming the valve as a fixed orifice device with a constant flow coefficient value (chosen as 0.0018 from the manufacturer).

Components in heating mode

DPR valve: Since the compressor in the TS-500 refrigeration unit is not operated using a variable-speed drive, the pressure ratio across the compressor cannot be varied arbitrarily using the compressor speed. Instead, the compressor is fixed at high or low speed to meet the desired capacity during heating mode, and the DPR valve is used to regulate the pressure ratio. By adjusting the valve opening, a backpressure is created, which drives the compressor to produce more work and provide more generated heat to the cargo space. Once the discharge pressure is settled, an iterative process is applied to compute the flow rate across the DPR valve, where the flow coefficient is a mapping function of the calculated mass flow rate. In this way, the pressure regulating performance is achieved as a result of valve opening changes. The development of the flow coefficient map can be found in Jain (2009).

Hot gas line: The hot gas line is a series of pipes that are engaged only in heating mode to connect the DPR valve outlet to the evaporator inlet. This component is modeled as a pressure drop element with heat transfer characteristics, and more modeling details are given in Jain (2009).

Modeling of refrigerant inlet conditions to evaporator during mode switch

Specific attention is paid here to the modeling of the evaporator inlet refrigerant flow rate and enthalpy due to their key effects on the system performance during the mode switching (Dopazo et al. 2010). The evaporator inlet flow is provided by the TXV in cooling mode, and then it is determined by the refrigerant flowing through the DPR valve and the hot gas line after the system switches to heating-mode operation. Equations 38 and 39 are used to describe the transients of the refrigerant inlet conditions during the mode switch by assuming the uniform mixing of two refrigerant flows, where

n is the number of parallel-passes in the evaporator:

$$\dot{m}_{i,e} = \frac{\dot{m}_v + \dot{m}_{dpr}}{n}, \tag{38}$$

$$h_{i,e} = \frac{\dot{m}_v h_{o,v} + \dot{m}_{dpr} h_{o,hgl}}{\dot{m}_v + \dot{m}_{dpr}}. \tag{39}$$

During heating-mode operation, the mass flow rate across the TXV bleed port is considered, as seen in Equation 38. In cooling-mode steady-state operation, the mass flow rate across the DPR valve is assumed to be zero.

Refrigerated cargo space model development

The refrigerated cargo space model introduced here accommodates the following important effects in food transportation: (i) varying ambient conditions, including ambient temperature, solar radiation intensity, and wind speed, and (ii) air infiltration. Three dynamic states, cargo space temperature T_{space}, interior surface temperature T_{is}, and exterior surface temperature T_{es}, are defined to describe the model dynamics, as shown in Equation 40. The cargo space air, interior, and exterior surface heat balance governing equations are presented in Equations 41–43 by applying energy conservation principles:

$$x = [T_{space}\ T_{is}\ T_{es}]^T, \tag{40}$$

$$\frac{dT_{space}}{dt} = \frac{\dot{Q}_{inconv} + \dot{Q}_{inf} - \dot{Q}_{vcc}}{(MC)_{air}}, \tag{41}$$

$$\frac{dT_{is}}{dt} = \frac{\dot{Q}_{cond} - \dot{Q}_{inconv}}{(MC)_{space,\,w}}, \tag{42}$$

$$\frac{dT_{es}}{dt} = \frac{\dot{Q}_{solar} - \dot{Q}_{outconv} - \dot{Q}_{cond}}{(MC)_{space,w}}. \tag{43}$$

The solar load $\dot{Q}_{solar}$ and air infiltration load $\dot{Q}_{inf}$ are computed from Equations 44 and 45. $\dot{Q}_{inconv}$ and $\dot{Q}_{outconv}$ represent the convective heat transfer from the surface to the air, and the heat conduction from the exterior to interior surface is given by $\dot{Q}_{cond}$. The VCC refrigeration system capacity provided to the cargo space is denoted as $\dot{Q}_{vcc}$. More information on the surface heat transfer coefficients and heat balance calculations can be found in Li et al. (2010):

$$\dot{Q}_{solar} = \beta I_{solar\_radiation}, \tag{44}$$

$$\dot{Q}_{inf} = V_{space}\rho_{space}c_{space}(T_{amb} - T_{space})(ACH). \tag{45}$$

Simulation environment

To simulate and validate the transport refrigeration system performance with cooling-/heating-mode switch operations, the component models described above, along with pipe models and hydraulic resistance elements (McKinley and Alleyne 2008a) connecting each component in the VCC system, are implemented in Thermosys (Rasmussen 2005), a Matlab/Simulink toolbox for simulation of dynamic thermal system models. The pipe models calculate pressure drops between any two components, and the hot gas line component is a variation of the pipe model. The inputs to each model are generally the outputs of other component models. For instance, the refrigerant inlet and outlet pressures are the TXV model inputs, yet they themselves are the outputs of the SLHX and the evaporator model, respectively. The refrigeration unit model is coupled to the cargo space with the airflow interactions as presented before. The cooling-/heating-mode switch temperature control algorithm is implemented using the Matlab/State-flow toolbox.

The refrigerant-side and air-side heat transfer coefficients are computed separately in the switched heat exchangers for the refrigeration system. The structure-to-air heat transfer coefficients are calculated by j-factor correlations (Kays and London 1984). The two-phase refrigerant-side heat transfer coefficients are defined by empirical equations. Specifically, the two-phase refrigerant heat transfer correlation developed by Dobson and Chato (1998) is chosen for the condenser, and the evaporator model uses the correlation from Wattelet et al. (1994). A Colburn modulus–Reynolds number correlation (Manglik and Bergles 1995) is applied for the single-phase refrigerant-side heat transfer coefficient calculation. When the system switches from cooling mode to heating mode, the two-phase heat transfer correlation shifts from the Wattelet correlation for evaporating flows to the Dobson–Chato correlation for condensing flows. More information about the numerical solution procedures of the switched heat exchangers is available in Li and Alleyne (2010).

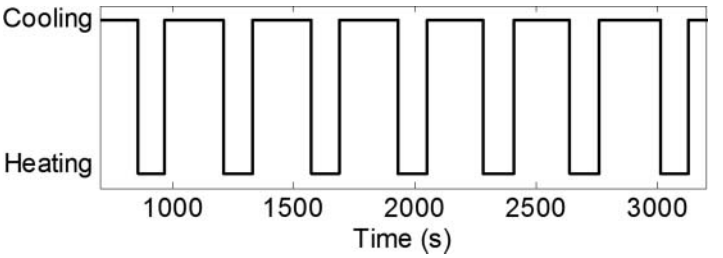

Figure 7. Model input: cooling/heating sequence for refrigeration unit validation.

Model validation

This section is divided into two parts. The developed refrigeration unit model as depicted in Figure 2 is compared against the test data collected on the experimental platform during mode switch cycling, where the refrigerant mass distribution among the components during transients is illustrated. Second, the temperature pull-down and regulation validation results are presented for the transport refrigeration temperature control system (see Figure 1b). The reader is encouraged to refer to Jain (2009) for the validation of the individual components in the TS-500 refrigeration unit.

Refrigeration unit model validation during mode switch cycles

To validate the model performance of cooling-/heating-mode switch operation, comparisons against a reference dataset are described in this section. The experimental data for validation is chosen from the low compressor speed temperature regulation test, and the cooling-/heating-mode switch cycle as shown in Figure 7 is regarded as the unit model input. Other model inputs include the evaporator and condenser air inlet temperatures as given in Figures 8 and 9. The initial operating conditions of the refrigeration unit are listed in Table 2.

The plots in Figures 10–12 compare the experimental results with various model outputs. When the system operation switches from cooling to heating mode, the superheated vapor exiting the compressor is redirected to enter the evaporator instead of the condenser coil, which results in heat exchanger pressure changes, as seen in Figures 10 and 11. Due to the cycling input of the evaporator air inlet temperature (also the cargo space temperature) in Figure 8, the evaporator air outlet temperature increases to exceed the inlet temperature during heating mode and drops back to the initial condition after the system cools down, as shown in Figure 12.

The condenser and evaporator pressures are two important variables to determine the refrigeration system performance during cooling-/heating-mode switch cycles, and the model tracks the dynamics of the pressures quite well considering the large cycling transients and the complexity of the system. The predicted evaporator pressure responds slightly faster than the experimental curve in Figure 11, especially when the system operation switches from heating to cooling mode. This is due to the sudden decrease of the evaporator inlet refrigerant flow rate and the less accurate predictions of the refrigerant-side heat transfer rates during such large transients. As presented in Figure 12, there are some differences between the model output and the experimental measurement due to the thermal time constants of

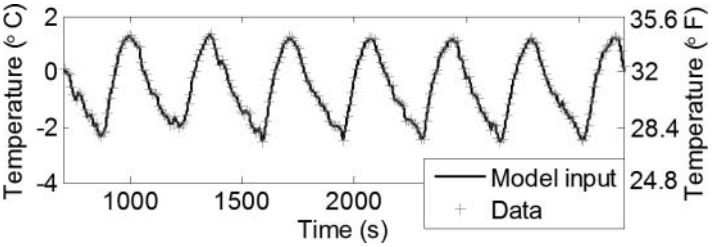

Figure 8. Model input: evaporator air inlet temperature for refrigeration unit validation.

Table 2. Refrigeration unit initial conditions for model validation.

	Units	Value
Evaporator		
Pressure	kPa (psi)	395 (57.29)
Refrigerant inlet enthalpy	kJ/kg (Btu/lb)	89.04 (38.28)
Air inlet temperature	°C (°F)	0.16 (32.29)
Air mass flow rate	kg/s (lb/min)	0.7 (92.59)
Refrigerant outlet superheat	°C (°F)	12 (21.6)
Accumulator		
Pressure	kPa (psi)	382.36 (55.46)
Refrigerant mass	kg (lb)	0.05 (0.11)
Compressor		
Inlet pressure	kPa (psi)	287.47 (41.69)
Outlet pressure	kPa (psi)	1726.5 (250.41)
Inlet temperature	°C (°F)	11.23 (52.21)
Outlet temperature	°C (°F)	82.7 (180.86)
Refrigerant mass flow rate	kg/s (lb/min)	0.051 (6.75)
Compressor speed	rpm	2520
Condenser		
Pressure	kPa (psi)	1726.5 (250.41)
Refrigerant inlet temperature	°C (°F)	82.7 (180.86)
Air inlet temperature	°C (°F)	26.05 (78.89)
Air mass flow rate	kg/s (lb/min)	0.75 (99.21)
Receiver tank		
Pressure	kPa (psi)	1655.39 (240.09)
Refrigerant mass	kg (lb)	0.53 (1.17)
TXV		
Inlet pressure	kPa (psi)	1650.53 (239.39)
Outlet pressure	kPa (psi)	395 (57.29)
Inlet temperature	°C (°F)	24.67 (76.41)
Valve opening (stroke)	mm (in.)	0.035 (0.0014)
Sensing bulb temperature	°C (°F)	–0.104 (31.81)
Refrigerant mass flow rate	kg/s (lb/min)	0.051 (6.75)
DPR valve		
Outlet pressure	kPa (psi)	395 (57.29)
Refrigerant mass flow rate	kg/s (lb/min)	0 (0)
Hot gas line		
Pressure	kPa (psi)	395 (57.29)
Refrigerant mass	kg (lb)	0.074 (0.16)

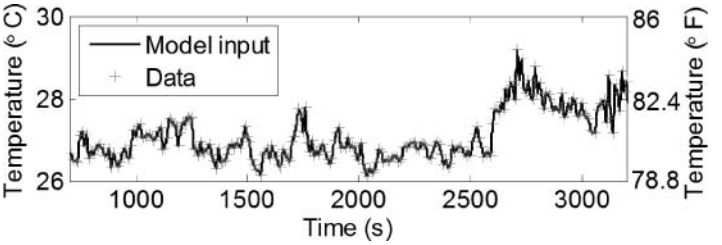

Figure 9. Model input: condenser air inlet temperature for refrigeration unit validation.

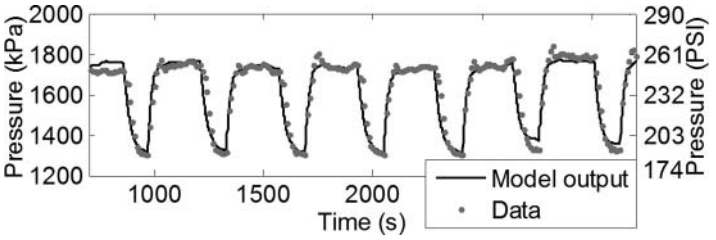

Figure 10. Model validation: condenser pressure.

the temperature sensors and steady-state model deviations. However, their shapes and trends are similar.

Figure 13 describes the switching transitions between different model representations in the evaporator model structure (see Figure 5) for this validation scenario, where relevant switching criteria are discussed in the section entitled "System modeling." In cooling mode, the evaporator is the two-zone (two-phase and superheated) model. When the system mode switch occurs, the normalized length of the superheated vapor zone is tracked until it becomes less than the switching threshold (0.5% of the total evaporator tube length), and the evaporator switches to the one-zone two-phase model and then moves to the superheated and two-phase two-zone model for heating-mode operation. When the system operation shifts back to cooling mode, a switch is triggered from the two-zone (superheated and two-phase) to the one-zone (two-phase) evaporator model, since the switching conditions described in Equations 27 and 28 are satisfied, and the pseudo-states are then applied to represent the dynamics of the inactive superheated inlet zone. Due to superheat regulation by the TXV in cooling mode, the superheated zone at the evaporator outlet becomes active, and the evaporator model switches back to the two-zone (two-phase and superheated) representation. Three repeated cooling-/heating-mode switch cycles are presented in Figure 14 to highlight the dynamic switching in terms of the length traces of three different zones (superheated, two phase, and superheated) in the evaporator during transients. The zone lengths (ζ_{e0}, ζ_{e1}, and ζ_{e2}) are dimensionless and normalized based on the total evaporator tube length to add up to one.

During cooling-mode operation, the condenser is a two-zone (superheated and two-phase) model configuration due to the existence of the receiver tank, maintaining its model representation during the mode switch transients, as shown in Figure 15. There is no refrigerant flow entering the condenser coil in heating mode, which leads to the decrease in length of the superheated vapor zone at the condenser inlet. Given longer durations for heating-mode operation, possible switches to different condenser model representations as presented in Li and Alleyne (2010) could occur. Figure 16 presents the dynamic switching in terms of the mean void fraction transients in the switched accumulator model (see Figure 6). The accumulator switches from the two-phase mixture in heating mode to the superheated vapor model in cooling mode, as the switching conditions given in Equations 31 and 32 are satisfied.

As mentioned previously, an advantage of the switched modeling techniques is the tracking of vapor and liquid refrigerant transients in the heat exchangers and the accumulator, which enables the calculation of refrigerant mass variations (Li et al. 2011). The refrigerant mass distribution among the system components during the mode switch

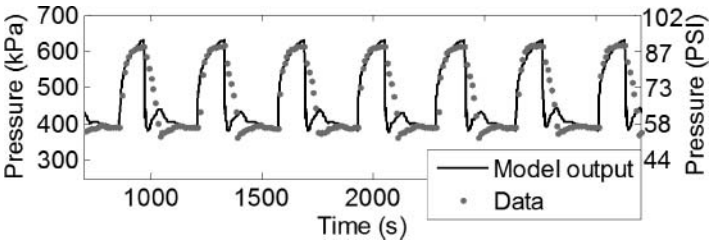

Figure 11. Model validation: evaporator pressure.

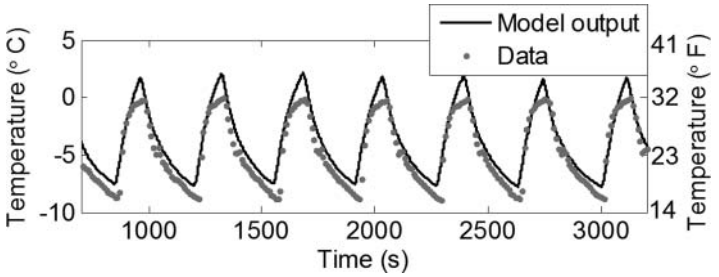

Figure 12. Model validation: evaporator air outlet temperature.

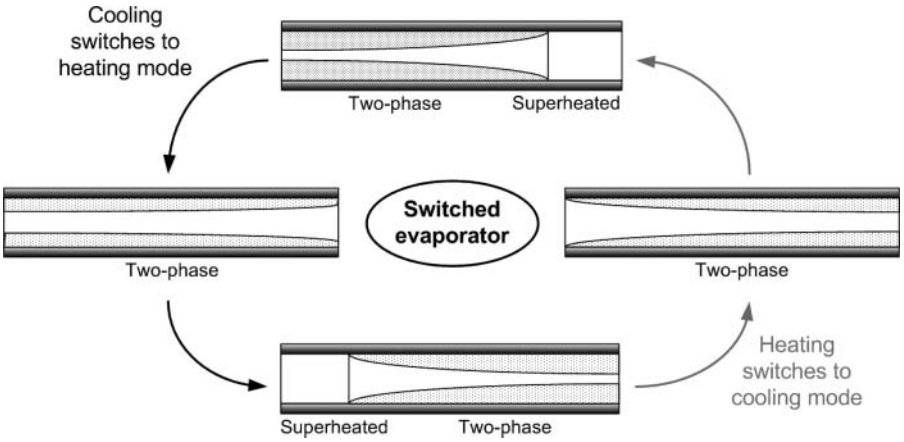

Figure 13. Switching transitions in the evaporator.

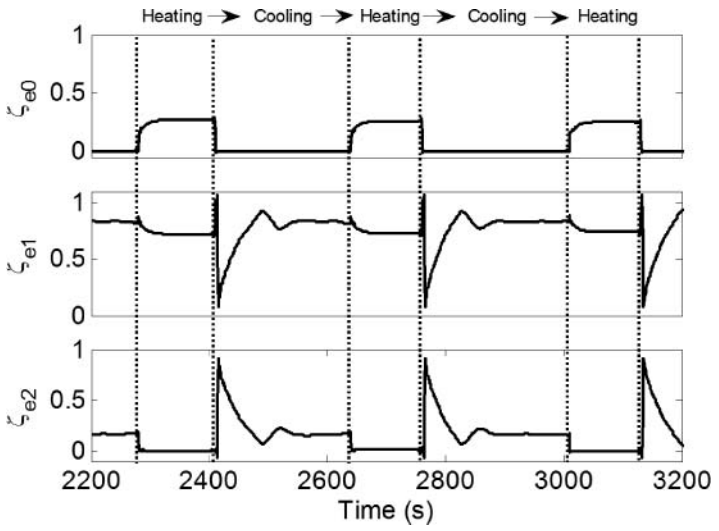

Figure 14. Evaporator superheated/two-phase/superheated zone length trace in transients.

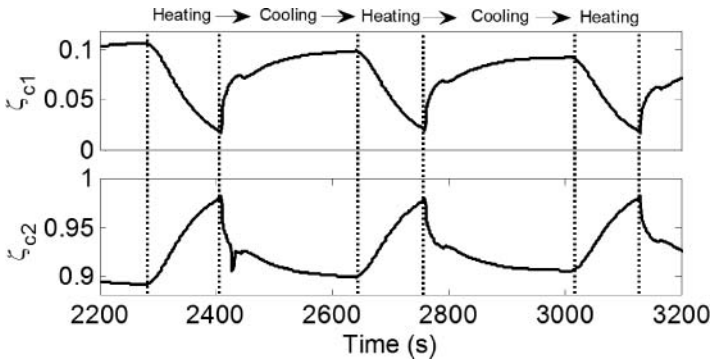

Figure 15. Condenser superheated/two-phase zone length trace in transients.

is explored based on the developed unit model, and three consecutive cycles are chosen again (see Figure 17) to illustrate the refrigerant mass migration in the high-side (condenser and receiver tank) and the low-side (evaporator and accumulator) components. When the system switches from cooling- to heating-mode operation, two-phase refrigerant flows through the SLHX and enters the accumulator, which results in the sudden increase of refrigerant mass inside the accumulator, as shown in Figure 17. During heating-mode operation, around 15% of the refrigerant mass in the high-side components migrates to the low side due to the bleed port effect of the TXV. When the system switches back to cooling-mode operation, the refrigerant mass is redistributed among different system components.

Refrigerated transport system validation with mode switch temperature regulation

The model validation scenario presented here, which is identical to the experimental study discussed in the "Experimental refrigeration system" section, includes a temperature pull-down and regulation test through cycling the system operation between cooling and heating mode. The temperature control objective is to maintain the cargo space temperature at the fresh set-point of –1.11°C (30°F) with an allowable variation of +2.5/–1.0°C (+4.5/–1.8°F). The schematic of the refrigeration unit temperature control system is presented in Figure 1b, and the ambient temperature as the system input is shown in Figure 18. The main cargo space model parameters for this study are given in Table 3.

With the cooling/heating temperature control algorithm, the resulting actuator performance in terms of compressor speed and cooling-/heating-mode switch cycles is given in Figures 19 and 20, respectively. The plot in Figure 21a compares the cargo space temperature with the measured experimental data, and a closer comparison between 10,000 and 12,000 sec is given in Figure 21b. As can be seen, the measured space temperature is drifting slightly below the set-point due to the varying cargo space thermal capacitance, which is not captured by the developed system model. However, overall the model predictions match the experimental results quite well in the time domain. The validation results further demonstrate the capability of the proposed dynamic modeling approach.

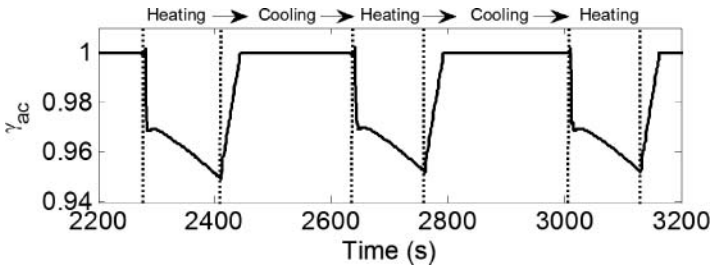

Figure 16. Mean void fraction variations in the accumulator in transients.

Table 3. Cargo space model parameters.

Variable	Definition	Value	Unit
$(MC)_{space,w}$	Cargo space wall thermal capacitance	100 (52.66)	kJ/K (Btu/°F)
$(MC)_{air}$	Air thermal capacitance inside the space	20 (10.53)	kJ/K (Btu/°F)
$(UA)_{space,w}$	Lumped heat transfer coefficient	0.095 (180.1)	kW/K (Btu/(h·°F))
A_{space}	Cargo space surface area	82.43 (887.27)	m^2 (ft^2)
V_{space}	Cargo space volume	38.62 (1363.9)	m^3 (ft^3)
β	Absorptivity to solar radiation intensity	0.12	
ACH	Air changes per hour	0.02	

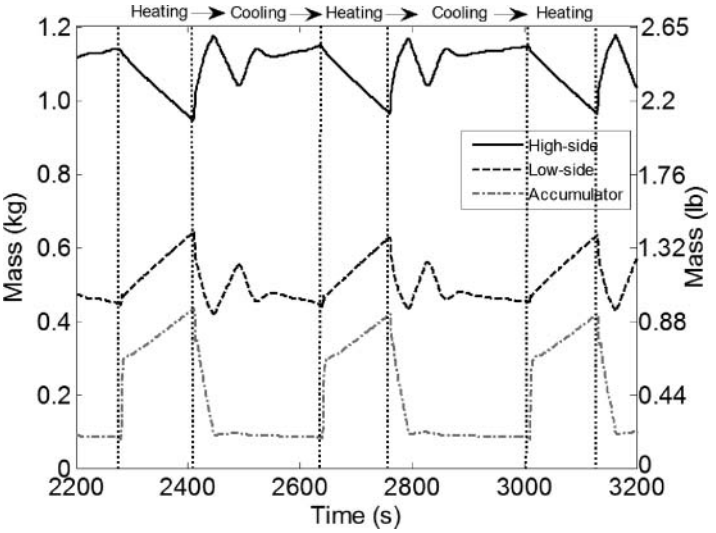

Figure 17. Refrigerant mass migration among system components in transients.

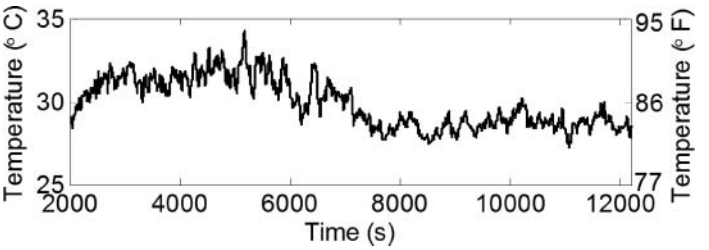

Figure 18. Ambient temperature for system input.

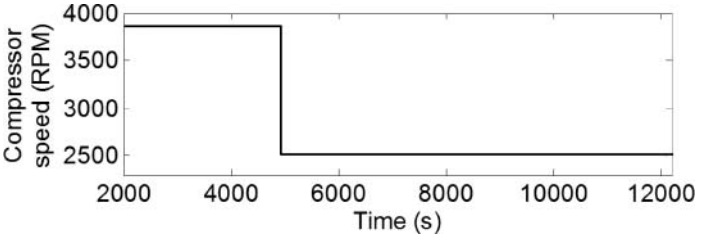

Figure 19. Compressor speed for temperature pull-down and regulation.

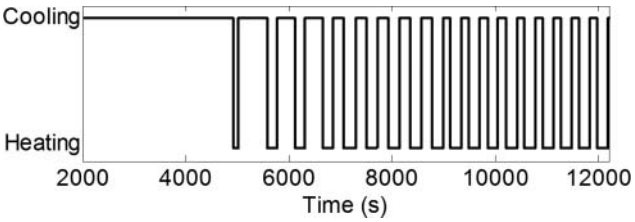

Figure 20. Cooling-/heating-mode switch cycles for temperature pull-down and regulation.

Case study

The validation results described above indicate that the developed transport refrigeration model is suitable for simulating the system operating characteristics during cooling-/heating-mode switch cycles. This section presents a case study on urban transport delivery to demonstrate the simulation capability in evaluating various models and scenarios. In the urban delivery application, customers

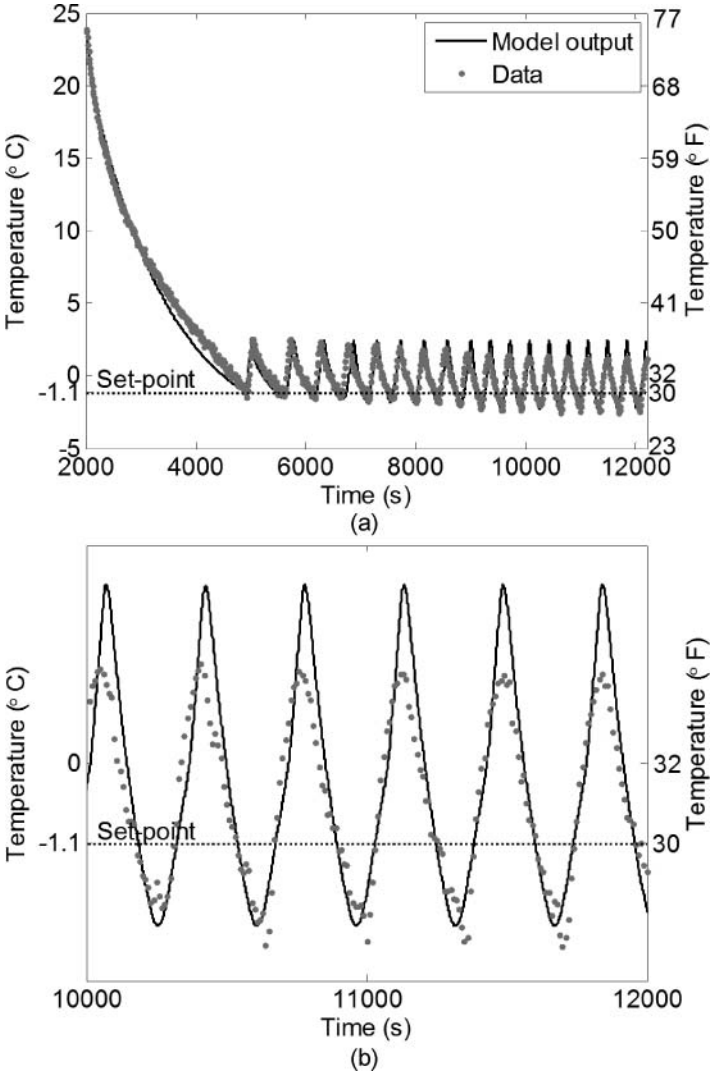

Figure 21. (a) Cargo space temperature performance during model validation and (b) zoomed-in plot for comparison.

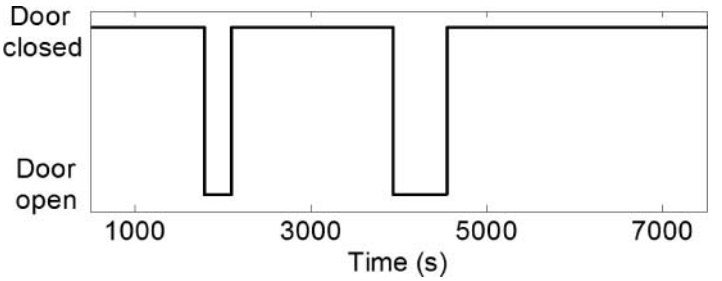

Figure 22. Door opening events for simulation input.

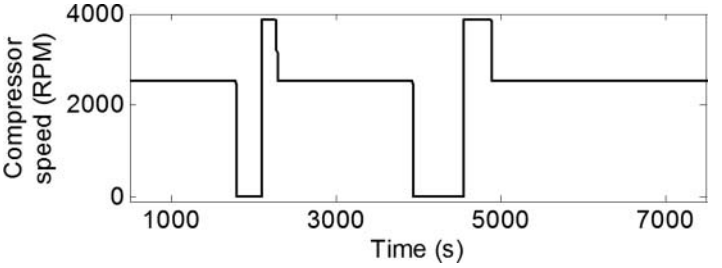

Figure 23. Compressor speed input to refrigeration unit.

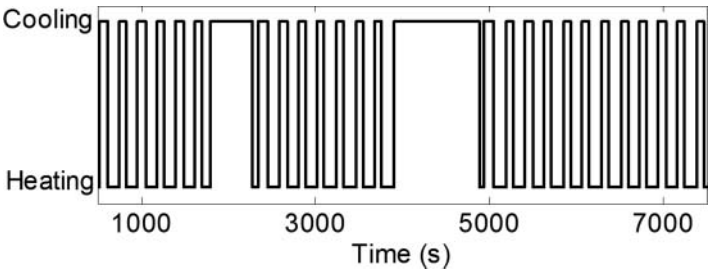

Figure 24. Cooling-/heating-mode switch cycles to refrigeration unit.

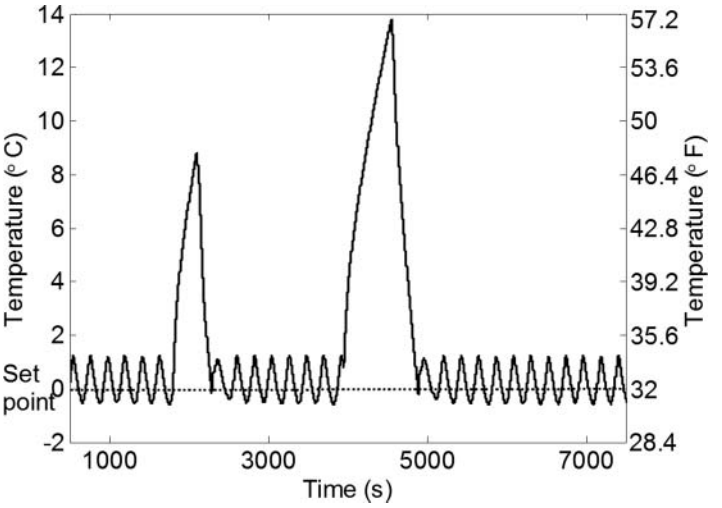

Figure 25. Cargo space temperature performance with effects of door-opening events.

typically have multiple stops with frequent door openings over the course of the day, and cooling-/heating-mode switching is preferably chosen for temperature regulation (Repice and Stumpf 2007). This case study introduces two door-opening events during operation, and the duration times are 5 and 10 min, respectively, as shown in Figure 22. The refrigeration system is assumed to be in the OFF condition during the door-opening event, and the cargo space temperature set-point is 0°C (32°F). Additionally, a constant ambient temperature (28°C [82.4°F]) is applied here. The interested reader is referred to Otten et al. (2010) for the validated refrigeration load calculations caused by the door openings.

After each door-opening event, the refrigeration system restarts with high compressor speed to cool down the cargo space temperature to the set-point, and then the system regulates the temperature with low-speed cycling between the cooling and heating modes of operation. The refrigeration unit inputs determined by the temperature control algorithm are shown in Figures 23 and 24, and the cargo space temperature performance is plotted in Figure 25. As illustrated, the presented modeling capability provides a tool for evaluating different scenarios, systems, and operation strategies prior to extensive experimental testing.

Conclusions and future work

This article presents dynamic modeling tools to capture system transient behavior during cooling-/heating-mode switch cycling operations in refrigerated transport systems. The Thermo King TS-500 transport refrigeration unit model in cooling- and heating-mode operation is introduced using the switched moving-boundary modeling approach proposed in Li and Alleyne (2010). The key components, evaporator and accumulator, are developed with switched model representations to accommodate the refrigerant phase changes that occur during the mode switch transients. The validation against experimental data shows that the system model is capable of predicting the system performance with cooling-/heating-mode switch temperature regulation. The results demonstrate the validity of the presented dynamic modeling approach in the simulation of the mode switch transients. Additionally, the refrigerated transport application case study shows the model benefits in performance predictions.

Finally, the results developed here provide a framework for examining dynamic modeling and management of defrost cycles in refrigeration systems. The capabilities of modeling the system behavior during cooling-/heating-mode switch operation provide the foundation to explore the system performance under cooling-/defrosting-mode switch cycles in refrigerated transport systems. Future steps would involve the coordination and co-simulation of frost formation and removal models with the refrigeration unit model. Different defrost control methods to determine the defrosting initiation condition and the defrosting operating time (Hewitt and Huang 2008) can then be implemented for system performance comparisons and optimization.

Acknowledgments

The support of this effort by Thermo King Corporation and the Air-Conditioning and Refrigeration Center (ACRC) at the University of Illinois at Urbana-Champaign is gratefully acknowledged.

Nomenclature

A	= area, m^2 (ft^2)
c	= specific heat, kJ/(kg·K) (Btu/(lb·°F))
C	= flow coefficient, dimensionless
f	= forcing function
h	= refrigerant enthalpy, kJ/kg (Btu/lb)
I	= solar radiation intensity, kW (Btu/h)
K	= gain in pseudo-state equations; set to 5.0, 1/s
$\dot{m}$	= mass flow rate, kg/s (lb/min)
MC	= thermal capacitance, kJ/K (Btu/°F)
NTU	= number of transfer units, dimensionless
P	= refrigerant pressure, kPa (psi)
$\dot{Q}$	= heat transfer rate, kW (Btu/h)
T	= temperature, °C (°F)
u	= input
V	= volume, m^3 (ft^3)
x	= state vector
$\tilde{x}$	= refrigerant vapor quality, dimensionless
Z	= coefficient matrix
α	= average heat transfer coefficient, kW/(m^2·K) (Btu/(h·ft^2·°F))
$\bar{\gamma}$	= mean void fraction, dimensionless

ζ = fraction of heat exchanger length covered by zone, called normalized zone length, dimensionless
η = efficiency, dimensionless
ρ = density, kg/m^3 (lb/ft^3)

Subscripts

ac = accumulator
amb = ambient
*c*1,*c*2, *c*3 = superheated, two-phase, sub-cooled zone in condenser
dpr = discharge pressure regulator valve
e = evaporator
*e*0, *e*1, *e*2 = superheated, two-phase, superheated zone in evaporator
*e*01 = boundary between superheated and two-phase zone in evaporator
*e*12 = boundary between two-phase and superheated zone in evaporator
etot = evaporation from given inlet two-phase refrigerant to saturated vapor
f = saturated liquid
g = saturated vapor
hgl = hot gas line
i = inlet
j = zone number; for evaporator, $j \in \{0, 1, 2\}$ (0 = superheated, 1 = two-phase, 2 = superheated)
k = compressor
o = outlet
slhx = suction line heat exchanger
v = expansion valve
w = heat exchanger structure (wall)

References

Akkerman, R., P. Farahani, and M. Grunow. 2010. Quality, safety and sustainability in food distribution: A review of quantitative operations management approaches and challenges. *OR Spectrum* 32(4):863–904.

Bendapudi, S., and J.E. Braun. 2002. A review of literature on dynamic models of vapor compression equipment. ASHRAE Report #4036–5. American Society of Heating, Refrigerating, and Air-Conditioning Engineers, Inc., Atlanta, GA.

Bendapudi, S., J.E. Braun, and E.A. Groll. 2005. Dynamic model of a centrifugal chiller system-model development, numerical study, and validation. *ASHRAE Transactions* 111(1):132–48.

Bendapudi, S., J.E. Braun, and E.A. Groll. 2008. A comparison of moving-boundary and finite-volume formulations for transients in centrifugal chillers. *International Journal of Refrigeration* 31(8):1437–52.

Byun, J.S., J. Lee, and C.D. Jeon. 2008. Frost retardation of an air-source heat pump by the hot gas bypass method. *International Journal of Refrigeration* 31(2):328–34.

Cecchinato, L., and F. Mancini. 2011. An intrinsically mass conservative switched evaporator model adopting the moving-boundary method. *International Journal of Refrigeration* 35(2):349–64. DOI: 10.1016/j.ijrefrig.2011.10.007.

Cho, H., Y. Kim, and I. Jang. 2005. Performance of a showcase refrigeration system with multi-evaporator during on-off cycling and hot-gas bypass defrost. *Energy* 30(10):1915–30.

Dobson, M.K., and J.C. Chato. 1998. Condensation in smooth horizontal tubes. *Journal of Heat Transfer* 120(1):193–214.

Dopazo, J.A., J. Fernandez-Seara, F.J. Uhía, and R. Diz. 2010. Modelling and experimental validation of the hot-gas defrost process of an air-cooled evaporator. *International Journal of Refrigeration* 33(4):829–39.

Eborn, J., H. Tummescheit, and K. Prölβ. 2005. Air conditioning—a Modelica library for dynamic simulation of AC systems. *Proceedings of the 4th International Modelica Conference, Hamburg-Harburg, Germany, March 7–8*.

He, X.D., S. Liu, and H.H. Asada. 1997. Modeling of vapor compression cycles for multivariable feedback control of HVAC systems. *Journal of Dynamic Systems, Measurement, and Control* 119(2):183–92.

Hewitt, N., and M.J. Huang. 2008. Defrost cycle performance for a circular shape evaporator air source heat pump. *International Journal of Refrigeration* 31(3):444–52.

Hoffenbecker, N., S.A. Klein, and D.T. Reindl. 2005. Hot gas defrost model development and validation. *International Journal of Refrigeration* 28(4):605–15.

Jain, N. 2009. Dynamic modeling and validation of a commercial transport refrigeration system. M.S. thesis, University of Illinois at Urbana-Champaign, Champaign-Urbana, IL. http://arg.mechse.illinois.edu/index.php?id=1144|ms.

James, S.J., C. James, and J.A. Evans. 2006. Modelling of food transportation systems—a review. *International Journal of Refrigeration* 29(6):947–57.

Jensen, J.M., and H. Tummescheit. 2002. Moving boundary models for dynamic simulations of two-phase flows. *Proceedings of the 2nd International Modelica Conference, Oberpfaffenhofen, Germany, March 18–19*.

Jolly, P.G., C.P. Tso, Y.W. Wong, and S.M. Ng. 2000. Simulation and measurement on the full-load performance of a refrigeration system in a shipping container. *International Journal of Refrigeration* 23(2):112–26.

Kapadia, R.G., J. Sanjeev, and R.S. Agarwal. 2009. Transient characteristics of split air-conditioning systems using R-22 and R-410A as refrigerants. *HVAC&R Research* 15(3):617–49.

Kays, W.M., and A.L. London. 1984. Chapter 2. *Compact Heat Exchangers*. New York: McGraw-Hill.

Koury, R.N.N., L. Machado, and K.A.R. Ismail. 2001. Numerical simulation of a variable speed refrigeration system. *International Journal of Refrigeration* 24(2):192–200.

Krakow, K.I., S. Lin, and L. Yan. 1993. An idealized model of reversed-cycle hot gas defrosting—Part 1: Theory. *ASHRAE Transactions* 99:317–38.

Li, B. 2009. Dynamic modeling and control of vapor compression cycle systems with shut-down and start-up operations.

M.S. thesis. University of Illinois at Urbana-Champaign, Champaign-Urbana, IL. http://arg.mechse.illinois.edu/index.php?id=1144|ms.

Li, B., and A.G. Alleyne. 2010. A dynamic model of a vapor compression cycle with shut-down and start-up operations. *International Journal of Refrigeration* 33(3):538–52.

Li, B., R. Otten, V. Chandan, W.F. Mohs, J. Berge, and A.G. Alleyne. 2010. Optimal on–off control of refrigerated transport systems. *Control Engineering Practice* 18(12):1406–17.

Li, B., S. Peuker, P.S. Hrnjak, and A.G. Alleyne. 2011. Refrigerant mass migration modeling and simulation for air conditioning systems. *Applied Thermal Engineering* 31(10):1770–9.

Liang, N., S. Shao, C. Tian, and Y. Yan. 2010. Dynamic simulation of variable capacity refrigeration systems under abnormal conditions. *Applied Thermal Engineering* 30(10):1205–14.

Limperich, D., M. Braun, G. Schmitz, and K. Prölβ. 2005. System simulation of automotive refrigeration cycles. *Proceedings of the 4th International Modelica Conference, Hamburg-Harburg, Germany, March 7–8*.

Liu, Z., G. Tang, and F. Zhao. 2003. Dynamic simulation of air-source heat pump during hot-gas defrost. *Applied Thermal Engineering* 23(6):675–85.

Manglik, R.M., and A.E. Bergles. 1995. Heat transfer and pressure drop correlations for the rectangular offset strip fin compact heat exchanger. *Experimental Thermal and Fluid Science* 10(2):171–80.

McKinley, T.L., and A. Alleyne. 2008a. Real-time modeling of liquid cooling networks in vehicle thermal management systems. Society of Automotive Engineers Technical Paper 01–0386, 2008 World Congress, Detroit, MI, USA, April 14–17.

McKinley, T.L., and A.G. Alleyne. 2008b. An advanced nonlinear switched heat exchanger model for vapor compression cycles using the moving-boundary method. *International Journal of Refrigeration* 31(7):1253–64.

Miller, W.A. 1987. Laboratory examination and seasonal analysis of frosting and defrosting for an air-to-air heat pump. *ASHRAE Transactions* 93:1474–89.

O'Neal, D.L., K. Peterson, N.K. Anand, and J.S. Schliesing. 1989. Refrigeration system dynamics during the reverse cycle defrost. *ASHRAE Transactions* 95(2):689–98.

Otten, R., B. Li, and A. Alleyne. 2010. Hardware-in-the-loop load emulation for air-conditioning and refrigeration systems. *13th International Refrigeration and Air Conditioning Conference, Purdue University, IN, July 12–15*.

Pettit, N., M. Willatzen, and L. Ploug-Sorensen. 1998. A general dynamic simulation model for evaporators and condensers in refrigeration. Part II: Simulation and control of an evaporator. *International Journal of Refrigeration* 21(5):404–14.

Qu, M., L. Xia, S. Deng, and Y. Jiang. 2012. A study of the reverse cycle defrosting performance on a multi-circuit outdoor coil unit in an air source heat pump—Part I: Experiments. *Applied Energy* 91(1):122–9.

Rasmussen, B.P. 2005. Dynamic modeling and advanced control of air conditioning and refrigeration systems. Ph.D. thesis. University of Illinois at Urbana-Champaign, Champaign-Urbana, IL. http://arg.mechse.illinois.edu/index.php?id = 1145|PhD.

Rasmussen, B.P., and A.G. Alleyne. 2004. Control-oriented modeling of transcritical vapor compression systems. *Journal of Dynamic Systems, Measurement, and Control* 126:54.

Repice, A., and A. Stumpf. 2007. Energy efficiency in transport refrigeration. *Proceedings of International Congress of Refrigeration, Beijing, China August 21–26*, paper no. ICR07-D2–362.

Shao, L.L., and C.L. Zhang. 2007. Logic unconstrained multi-zone evaporator and condenser models. *International Journal of Refrigeration* 30(5):926–31.

Tassou, S.A., G. De-Lille, and Y.T. Ge. 2009. Food transport refrigeration-approaches to reduce energy consumption and environmental impacts of road transport. *Applied Thermal Engineering* 29(8–9):1467–77.

Tso, C.P., Y.W. Wong, P.G. Jolly, and S.M. Ng. 2001. A comparison of hot-gas by-pass and suction modulation method for partial load control in refrigerated shipping containers. *International Journal of Refrigeration* 24(6):544–53.

Vaclavek, L., J. Lohan, and A. Ryan. 2003. Development and optimization of temperature control during reverse cycle and heating in a multi-zone refrigeration system. *Eurotherm Seminar 72, Thermodynamics, Heat and Mass Transfer of Refrigeration Machines and Heat Pumps, Valencia, Spain, March 31–April 2*.

Wattelet, J.P., J.C. Chato, B.R. Christoffersen, J.A. Gaibel, M. Ponchner, P.J. Kenney, R.L. Shimon, T.C. Villaneuva, N.L. Rhines, K.A. Sweeney, D.G. Allen, and T.T. Hershberger. 1994. *Heat transfer flow regimes of refrigerants in a horizontal-tube evaporator*. Air-Conditioning and Refrigeration Center TR-55, University of Illinois at Urbana-Champaign, Champaign-Urbana, IL.

Zhang, W.J., and C.L. Zhang. 2006. A generalized moving-boundary model for transient simulation of dry-expansion evaporators under larger disturbances. *International Journal of Refrigeration* 29(7):1119–27.

Zhang, W.J., C.L. Zhang, and G.L. Ding. 2009. Transient modeling of an air-cooled chiller with economized compressor. Part I: Model development and validation. *Applied Thermal Engineering* 29(11):2396–402.

Zivi, S.M. 1964. Estimation of steady-state steam void fraction by means of the principle of minimum entropy production. *Journal of Heat Transfer* 86:247–52.